ACS APPLIED MATERIALS & INTERFACES

Research Article

www.acsami.org

Using Confined Self-Adjusting Carbon Nanotube Arrays as High-Sensitivity Displacement Sensing Element

Jae-Ik Lee, Youngkee Eun, Jungwook Choi, Dae-Sung Kwon, and Jongbaeg Kim*

School of Mechanical Engineering, Yonsei University, 50 Yonsei-ro, Seodaemun-gu, Seoul 120-749, Republic of Korea

Supporting Information

ABSTRACT: Displacement sensing is a fundamental process in mechanical sensors such as force sensors, pressure sensors, accelerometers, and gyroscopes. Advanced techniques utilizing nanomaterials have attracted considerable attention in the drive to enhance the process. In this paper, we propose a novel and highly sensitive device for detecting small displacements. The device utilizes the changes in contact resistance between two sets of vertically aligned carbon nanotube (CNT) arrays, the growth of which was confined to enable their facile and reliable integration with fully fabricated microstructures. Using the displacement transduction of the proposed device, we successfully demonstrated a 3-axis wide bandwidth accelerometer, which was experimentally confirmed to be highly sensitive compared to conventional piezoresistive sensors. Through a test involving 1.2 million cycles of displacement transductions, the contact resistance of the CNT arrays was proved to be excellently stable, which was a consequence of the high electrical stability and mechanical durability of the CNTs.

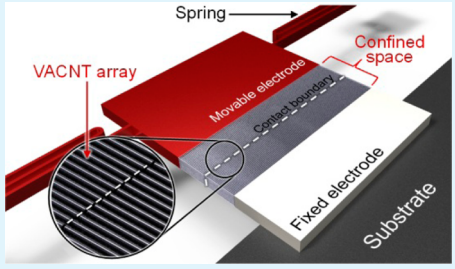

KEYWORDS: *carbon nanotube, confined growth, self-adjustment, displacement sensing, 3-axis accelerometer*

INTRODUCTION

Micromachined mechanical sensors are widely utilized in various industrial fields. They are applied, for example, in the inertial sensors of airbag restraints, pressure sensors of combustion engines, tactile sensors of artificial skin, and flow sensors for controlling equipment. Although diverse types are available, the sensing principles of most are based on the conversion of a mechanical load into displacement or accumulated strain. The displacement or strain is then transformed into an electrical signal, and subsequently into various physical parameters such as force, pressure, angular rate, acceleration, flow rate, and tactile information, depending on the purpose of the sensor.[1−6] The characteristics of micromachined mechanical sensors are mainly determined by employed displacement or strain sensing mechanisms. For example, micromachined mechanical sensors utilizing capacitive displacement sensing have the advantages of high sensitivity and low power consumption. They are, however, sensitive to electromagnetic interference, owing to the high impedance of the capacitivity-sensing node.[7] Micromachined mechanical sensors that utilize piezoresistive strain sensing are characterized by a simple structure, simple fabrication process, and simple read-out circuitry. Low sensitivity is, however, their primary disadvantage.

The demand for enhanced performance of micromachined mechanical sensors has prompted significant effort toward the development of displacement and strain sensors utilizing new materials and sensing mechanisms. Carbon nanotubes (CNTs) have attracted much interest in this drive, considering their exceptional electrical and mechanical properties, which include high mechanical strength,[8−10] good electrical conductivity,[11,12] and resistance to wear.[13] The electromechanical displacement sensing ability of an individual CNT has been studied by several researchers,[14−17] and an unusually high gauge factor (GF) of 2900 has been reported.[14] However, the fabrication of displacement sensors utilizing a single CNT is time-consuming and expensive owing to the lack of scalable integration methods.

The electromechanical characteristics of vertically aligned CNT (VACNT) arrays when displaced or under strain have also been studied and documented.[18−23] VACNT arrays can be repeatedly and significantly compressed without structural failure,[18,19] which affords a reliable electrical path. Single-walled VACNT arrays of length 600 nm also show a conductance change of about 12% when displaced by 120 nm.[20] Moreover, a macroscopic block of VACNTs exhibits a 52% increase in conductivity under 45% compressive strain.[21] VACNTs supported by a deflectable polymer membrane have also been used as strain sensors with a GF of 4.52 and maximum detectable strain of 1.5%.[22] Recently, micromachined mechanical sensors utilizing the deformation of VACNTs have been proposed for application in pressure, tactile, and vibration sensors.[23] The electrical resistance of VACNTs in such sensors decreases to 35% under a strain of 10%, which affords a GF of 3.5. Although mechanical transducers utilizing VACNT arrays can be fabricated by a relatively facile process, their sensitivities are much lower than those of single-CNT-based transducers.

Received: March 13, 2014
Accepted: June 10, 2014
Published: June 10, 2014

   dx.doi.org/10.1021/am5015138 | ACS Appl. Mater. Interfaces 2014, 6, 10181−10187

Additionally, the reproducible fabrication of VACNT-based sensors is challenging, which limits their practical usage.

We propose a new approach to utilizing VACNT arrays as the sensing element of a displacement sensor. The sensing principle is based on changes in the electrical contact resistance between the VACNT arrays. The proposed sensing system is based on self-adjusting facile contact between VACNTs, which affords the integration of the VACNTs with fully fabricated microstructures. Like piezoresistive transducers, the proposed displacement sensor employs simple read-out circuitry based on a conventional resistive bridge. It also has the advantage of offering freedom in designing the mechanical structure, unlike a piezoresistive transducer, which requires the placement of the sensing element at highly strained locations. Although relatively low sensitivity is the major disadvantage in piezoresistive transducer, the proposed VACNT-based displacement sensor exhibits outstanding sensitivity by means of a novel sensing mechanism.

RESULTS AND DISCUSSION

Figure 1a is a schematic of the proposed VACNT-based displacement sensor. The silicon microstructures including a fixed and a movable electrode are formed by standard silicon processing techniques. The two sets of VACNT arrays are synthesized in a confined space between the electrodes. (The detailed fabrication process is presented in Figure S1 in the Supporting Information.) Scanning electron microscopy (SEM) images of the VACNT-filled gap between the electrodes and an enlarged image of the VACNTs are shown in Figure 1b,c. Catalytic chemical vapor deposition (CVD) is used to synthesize the well-aligned CNTs. When two sets of growing VACNT arrays meet each other at the middle of the confined space, they form a contact boundary, as shown in Figure 1b. Even if synthesis continues, the dense VACNT arrays maintain the contact boundary without penetrating each other, owing to the strong van der Waals interaction within them.[24−26] Eventually, the arrays self-adjust their lengths to half of the gap between the two electrodes. Figure 1d shows the self-adjusting characteristics of the VACNTs. As can be clearly seen, the VACNTs in the confined space (Region A) are shorter than those grown without confinement (Region B). The confined growth enables the reproducible fabrication for displacement sensors with the designed length of the CNTs. In addition, the length-adjusting characteristic of our confined growth process also enables the synthesis of CNT arrays of various lengths by a single CVD process. Figure 1e shows VACNTs synthesized in a nonuniform gap between the silicon microstructures. Removal of the mating part clearly shows that the height of the VACNT array varies with the gap (Figure 1f). Several approaches have been employed in the effort to control the length of VACNTs in stationary structures.[27−29] We utilized an improved and more advanced approach, which involved the facile and scalable integration of the length-controlled VACNTs with the suspended parts of the fully fabricated 3D microstructures.

Figure 2 is a schematic of the displacement transduction mechanism through contacting VACNT arrays. As can be seen, the relatively long CNTs (colored red) are in contact with those from the opposite electrode, whereas the shorter CNTs (colored black) remain detached after completion of the confined growth. As shown in Figure 1c, the CNTs are buckled and zigzagged from the confined growth. When the movable electrode moves away from the fixed electrode (the separation mode shown in Figure 2b), the CNTs in contact are

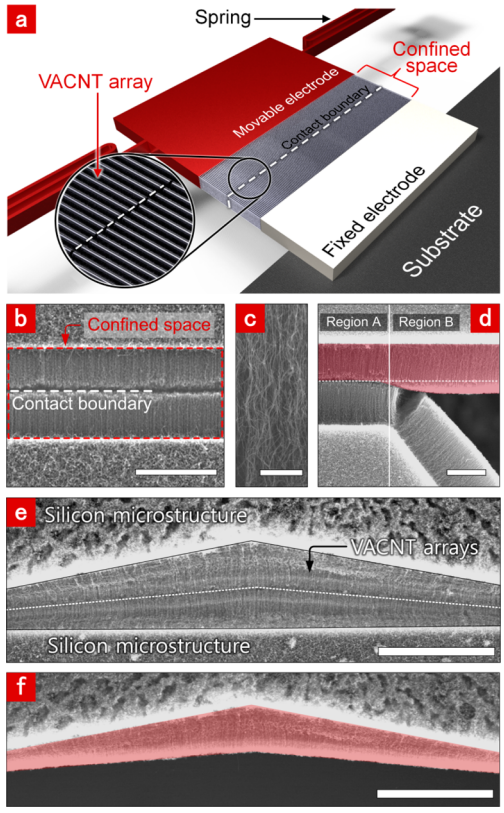

Figure 1. VACNT-based displacement sensor and confined growth of VACNTs (a) Schematic of structure of VACNT-based displacement sensor, showing two sets of aligned CNT arrays in contact between the fixed and movable electrodes. (b) SEM image of VACNT arrays grown in the confined space between the two electrodes. Scale bar: 10 μm. (c) Enlarged SEM image of VACNTs showing their buckled shape. Scale bar: 1 μm. (d) SEM image showing VACNTs in the confined space (Region A). The portion artificially colored red compares their short length with that of VACNTs grown without confinement (Region B). Scale bar: 10 μm. (e,f) SEM images of two sets of VACNT arrays synthesized in the nonuniform gap. The heights of the VACNT arrays vary with the gap (artificially colored red). Scale bar: 20 μm.

straightened by the adhesion force between them, and are sequentially detached from the shortest to the longest. Consequently, the number of CNTs maintaining contact is gradually reduced, and the overall contact resistance gradually increases. Conversely, when the movable electrode approaches the fixed one (the approach mode shown in Figure 2c), contacts are sequentially formed between CNTs from the longest to the shortest, which gradually decreases the contact resistance. Sliding displacement, in which the movable electrode moves in a direction parallel to the fixed one without a change in the gap between the two, can also be transduced into electrical signals. As depicted in Figure 2d, when the movable electrode moves in this manner (sliding mode), the area of the overlapping CNT contact for the flow of electrical current decreases and the electrical resistance increases.

To demonstrate the displacement sensing capability, the change in the electrical contact resistance between the two sets of VACNT arrays was monitored when two electrodes initially separated by 8 μm were separated further and then brought closer beyond the initial separation. The displacement of the movable electrode was achieved by a piezoelectric actuator with a resolution of 120 nm. Figure 3a is a plot of the measured

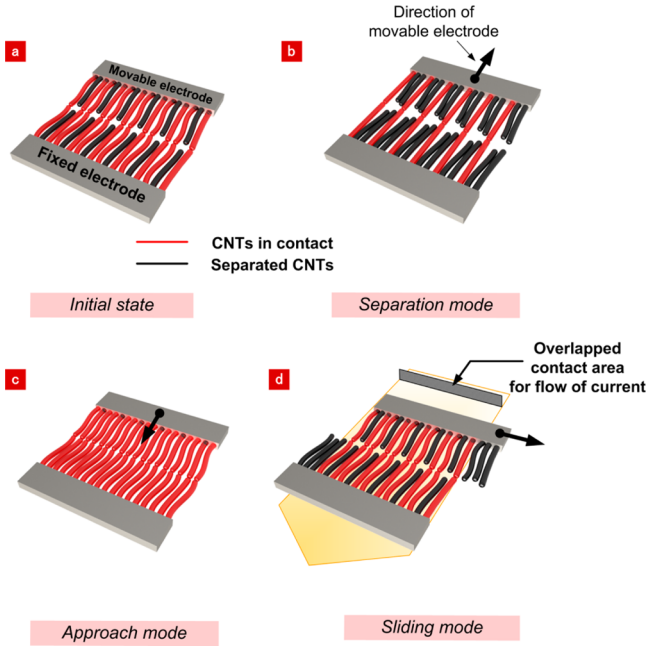

Figure 2. Displacement transduction mechanism. (a) Schematic of structure of VACNT-based displacement sensor in the initial state, in which the relatively long CNTs are in contact and the shorter ones are separated. (b,c) In the separation and approach modes, the number of CNTs in contact varies with the gap, resulting in a change in the contact resistance. (d) In the sliding mode, the overlapping contact area of the VACNTs when electrical current is flowing varies with the displacement of the movable electrode.

change in contact resistance in the separation mode against the displacement for three cycles. The measured electrical resistance monotonically increases as the movable electrode is gradually separated from the fixed electrode. Particularly, for a displacement below 1 μm, highly reproducible signals with very little hysteresis are observed, as shown in the inset in Figure 3a. The sensor exhibits remarkable sensitivity to even very small displacements. For a 1.8 μm displacement of the movable electrode, the electrical contact resistance changes from 3.6 kΩ to more than 2 MΩ. This drastic change in electrical resistance corresponds to a GF of up to 3115 (Figure S2, Supporting Information), which exceeds previously reported GFs of single CNT-based mechanical sensors (~2900),[14] as well as conventional piezoresistive sensors utilizing metal strain gauges (1−5) and silicon semiconducting strain gauges (80−200).[30] The maximum sensing range in the separation mode is 2.1 μm, which corresponds to the complete separation of the contacting CNTs (Figure 3b). When the gap is reduced, the separated CNTs re-establish contact at a displacement of 1.8 μm. The discrepancy of 0.3 μm in the sensing range is due to the buckled shape of the CNTs. As mentioned earlier, when the gap is gradually increased from the initial state, the contacting buckled CNTs are straightened. After complete separation, the elasticity of the CNTs restores the original buckled shape and re-establishes electrical contact at a displacement of 1.8 μm, which is 0.3 μm less than the initial separation of 2.1 μm.

For each pair of contacting CNTs, electrical resistance changes initially from the buckle straightening, and subsequently from the separation. However, due to the deviation in the buckled length and total length of each CNT, it is presumed that both the buckle straightening and the separation of individual CNTs would contribute the change in electrical resistance simultaneously throughout the most of the sensing range, and thus abrupt change in the slope is not observed.

Figure 3c shows the measured change in contact resistance in the approach mode for three cycles. A negative displacement indicates that the direction of the movable electrode is opposite to that of the separation mode. The change in resistance in the sensing mode is reproducible down to a displacement of −1.2 μm from the initial state, implying that the CNTs are elastically deformed. However, for displacements below −1.2 μm, the CNT arrays do not fully recover their initial contact resistance owing to their permanent deformation. The data of the separation and approach modes are both plotted for the same resistance scale in Figure 3d, in which the nonlinear resistance change of the displacement transducer fits well as an exponential curve. The increasing slope indicates that the number of contacting CNTs decays exponentially as the gap between the two electrodes increases. The effective differential sensitivity σ_R (defined as $\sigma_R = [dR/dz]|z$, where R is the electrical resistance for a given displacement z)[14] determined from the exponential fit, is 429 Ω/nm at $z = -0.96$ μm (approach mode) and 439 kΩ/nm at $z = +0.96$ μm (separation mode). The changes in electrical resistance are also affected by the piezoresisitivity of individual CNTs[14] and cross-tube coupling within arrays,[23] as well as the contact resistance change between CNT arrays. However, because diffusive electrical transport in CNTs is much more efficient compared to that at the contact between CNTs, the total electrical resistance is dominated by the contact resistance, and changes in electrical resistance owing to the piezoresisitivity of individual CNTs and cross-tube coupling within arrays are negligible.[32,33] The presented sensor gives much higher sensitivity compared to other CNT array-based mechanical sensors without a contacting scheme (Figure S2, Supporting Information), which also implies that contact resistance change is the dominant phenomenon of the transduction.

For the displacement of 0.96 μm in the separation mode, the increase in the electrical contact resistance is about 30 times the initial resistance. Considering that the electrical contact resistance is inversely proportional to the number of contacting CNTs, this result indicates that the number of contacting CNTs decreased to 1/30 (less than 4%). The drastic change in the number of contacting CNTs, as well as the outstanding sensitivity, can be attributed to the small deviation in the length of CNT arrays. Previous report shows that the deviation in length of CNTs is getting smaller with the decrease of the average length of CNTs.[34] Since smaller deviation in CNT lengths results in larger change in number of contacting CNTs with respect to a unit displacement, the sensor with shorter average length of CNTs would possibly have higher sensitivity and smaller sensing range. In addition, the confined growth ensures that the CNTs have similar height since the growth is always terminated at the center of the gap, hence the reproducibility of the sensing function of the device. The remarkable sensitivity to even a very small displacement in both separation and approach modes could be harnessed for various mechanical sensors, considering the ongoing efforts for miniaturization of sensors and the lack of scalable measurement method.[14]

To demonstrate the displacement sensing ability of the device in the sliding mode, we fabricated the test platform shown in Figure 4a. The movable part (artificially highlighted in blue) of the test platform consists of a shuttle and an electrostatic actuator[31] used to produce displacement. The

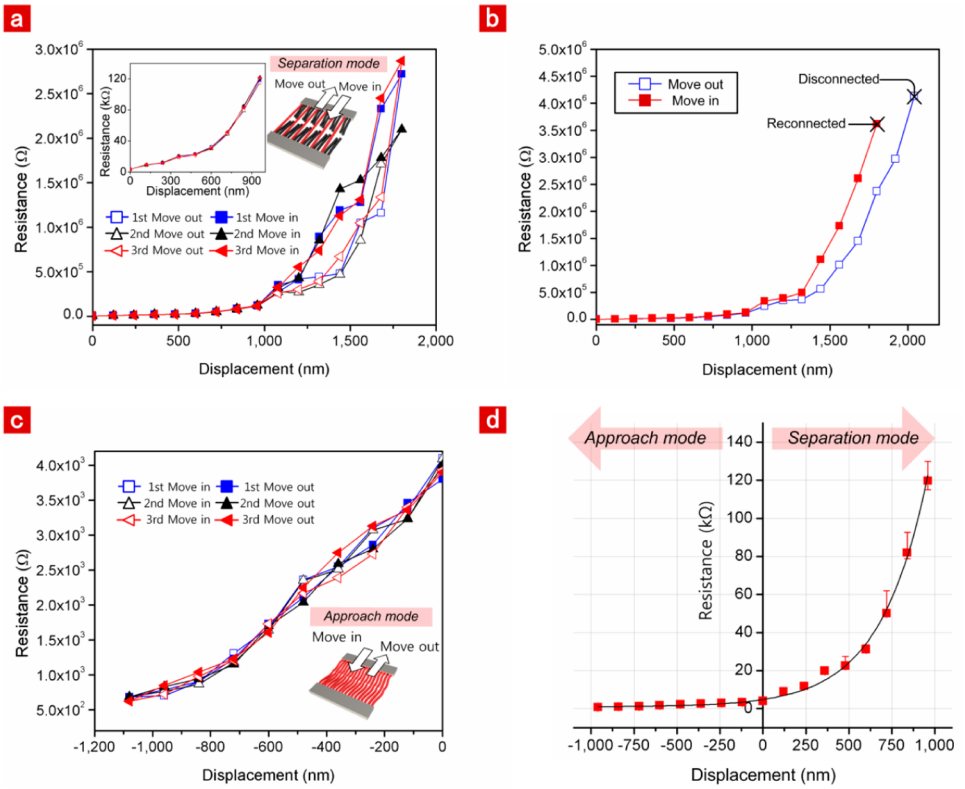

Figure 3. Electromechanical characterization of separation and approach modes. (a) Change in electrical contact resistance in the separation mode over three cycles. The inset shows that the signals of the sensing mode are highly reproducible and there is very little hysteresis for displacements below 1 μm. (b) Change in electrical contact resistance in the separation mode beginning at when the movable electrode is separated from the fixed electrode, through when the CNTs are completely separated, and up to when they return to their original positions. (c) Change in electrical contact resistance in the approach mode over three cycles. (d) Change in electrical contact resistance in both modes with exponential fit.

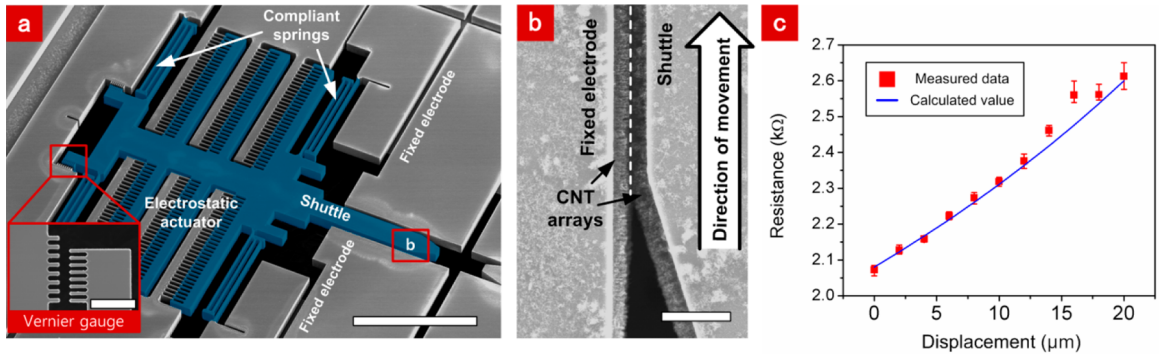

Figure 4. Electromechanical characterization of sliding mode. (a) SEM image of platform fabricated to characterize the sliding mode. The VACNT arrays are synthesized between the two fixed electrodes and the movable shuttle. The movable part (artificially colored blue) consists of compliant springs, a shuttle, and an electrostatic actuator for producing displacement. Scale bar: 500 μm. (b) SEM image of VACNT arrays between the fixed electrode and the shuttle. Scale bar: 15 μm. (c) Change in electrical contact resistance in the sliding mode.

shuttle of the movable part is positioned between two fixed electrodes, and the VACNT arrays are synthesized on the side walls of the shuttle and the fixed electrodes (Figure 4b). A constant bias voltage of 5 V is applied between the two fixed electrodes and the change in electrical contact resistance between the contacting VACNT arrays is monitored as the shuttle is moved by electrostatic force. The displacement of the shuttle is optically measured through the integrated vernier gauge shown in the inset in Figure 4a. As illustrated in Figure 2d, the sensing mechanism in the sliding mode is based on changes in the overlapping contact area between the VACNT arrays. This change in area is directly proportional to the displacement of the shuttle and proportional to the electrical current (Figure S3, Supporting Information). Thus, the displacement of the shuttle can be easily estimated by monitoring the change in contact resistance in the sliding mode. As shown in Figure 4c, the calculated resistances (solid line) agree well with the measured resistances (squares). The sensitivity in the sliding mode is quite lower than those in the separation and approach modes. However, the sensitivity and sensing range in the sliding mode can be easily tuned by altering the initial contact length between the two VACNT arrays (Figure S4a, Supporting Information). Additionally, the sensible range of the displacement is much wider than those in

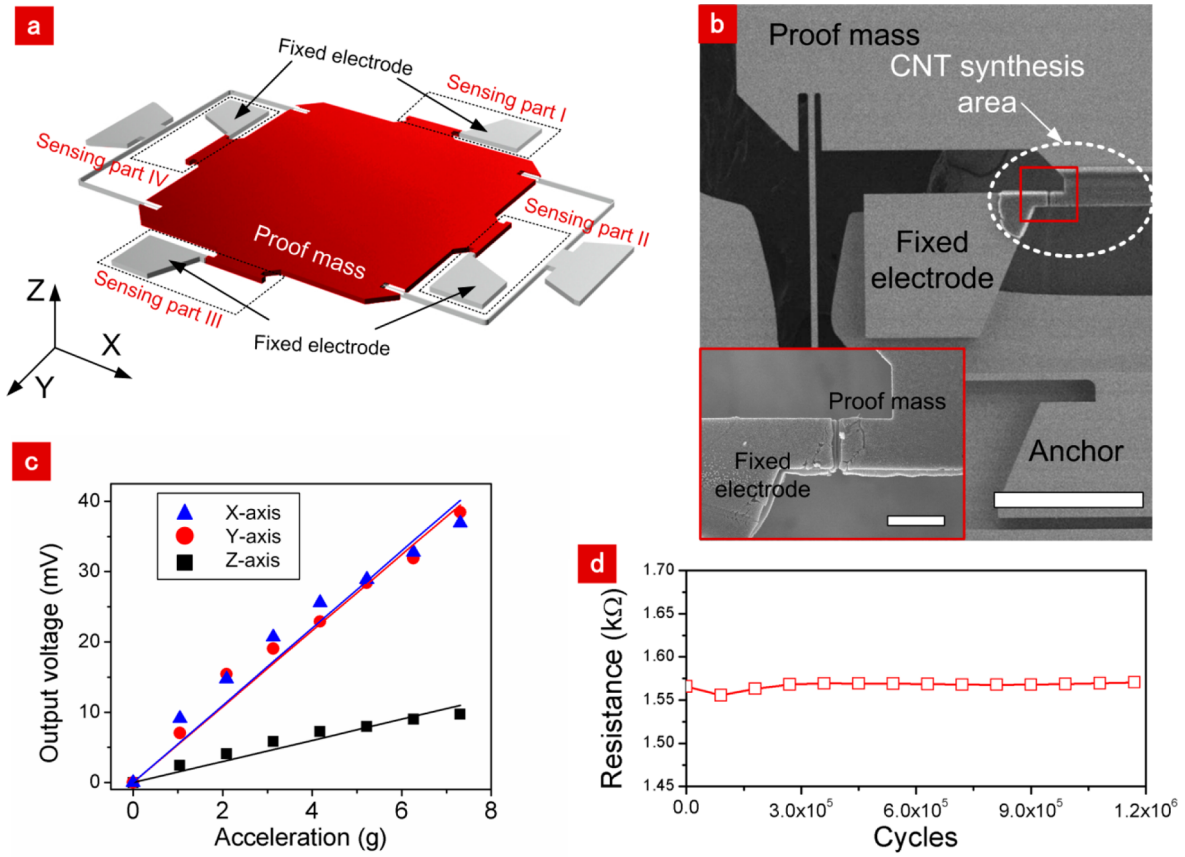

Figure 5. 3-Axis accelerometer utilizing the VACNT-based displacement sensor. (a) Schematic of the 3-axis accelerometer, comprising a monolithic proof mass, springs, and four sensing parts. (b) SEM image of fabricated accelerometer. Scale bar: 500 μm (scale bar of the inset: 50 μm). (c) Sensing characteristics of proposed accelerometer. (d) Reliability test results for a sinusoidal acceleration of frequency 300 Hz and magnitude −5 to +5 g using 1.2 million cycles.

the separation and approach modes. We conducted displacement sensing up to 2000 μm (Figure S4b, Supporting Information), but the sensing range can still be widened as long as there is a parallel gap of sufficient length.

To verify the potential of the proposed displacement transduction for use in mechanical sensors, we demonstrated acceleration sensing. The first demonstration involved a 1-axis accelerometer (Figure S5, Supporting Information). High sensitivity and resonant frequency, and hence a wide bandwidth, were simultaneously achieved, which is difficult in conventional piezoresistive acceleration sensors, in which increased sensitivity is achieved at the expense of bandwidth. The sensitivity and bandwidth can be further improved by the modification of the positions of the VACNT arrays. We extended the 1-axis accelerometer design to 3-axis acceleration sensing by combining the separation, approach, and sliding modes on a single proof mass. Figure 5a is a schematic of the sensor. The 3-axis accelerometer consists of a monolithic proof mass, springs to allow movement of the proof mass in the x, y, and z directions, and four sensing parts. In each sensing part, two sets of vertically aligned CNTs are grown from the surfaces of the proof mass and the fixed electrodes facing each other. To avoid the formation of an undesirable electrical path, an iron catalyst is selectively deposited in a predesignated area using a shadow mask, which ensures that the CNTs are synthesized only in the sensing area as shown in Figure 5b.

For acceleration in the $-x$ direction, the electrical contact resistance of the VACNT arrays of the proposed accelerometer decreases in sensing part I (approach mode) and increases in sensing part III (separation mode). At the same time, in sensing parts II and IV, the resistance of the two sensing electrodes increases in the sliding mode. For lateral accelerations in the $+x$ and $\pm y$ directions, similar behaviors are observed; only one sensing part shows decreased contact resistance, whereas the other three parts exhibit increased contact resistance. For vertical acceleration in the z-direction, increase in the contact resistance is monitored by all sensing parts in the sliding mode. The direction and magnitude of the acceleration can therefore be detected by monitoring the change in electrical contact resistance in each sensing part. In Figure S6 in the Supporting Information, the resistance changes in the different sensing parts with respect to the direction of acceleration are summarized. The changes in each sensing part with respect to the applied acceleration are linearly fitted in Figure 5c. The sensitivities calculated from the linear fit are 0.640 mV/g/V in the x-direction, 0.592 mV/g/V in the y-direction, and 0.300 mV/g/V in the z-direction. The first resonant frequency of the accelerometer is observed to be 2.572 kHz. Owing to the high sensitivity of the VACNT-based displacement transducer, the proposed 3-axis accelerometer exhibited both higher sensitivity and higher resonant frequency than typical piezoresistive 3-axis accelerometers (Figure S7, Supporting Information). To check for the possibility of contact degradation from repetitive mechanical contact, we performed a reliability test. For a sinusoidal acceleration of frequency 300 Hz and magnitude −5 to +5 g, the change in contact resistance was monitored and

dx.doi.org/10.1021/am5015138 | ACS Appl. Mater. Interfaces 2014, 6, 10181−10187

plotted (Figure 5d). Over the 1.2 million cycles of the test, the deviation of the contact resistance from the initial value was less than 1%. The high electrical stability and mechanical durability are attributed to the outstanding bending elasticity, robustness, and wear resistance of CNTs, as reported in previous studies.[8−10,13,18,19]

CONCLUSION

We have proposed and described a new approach to transducing displacement into electrical signals. The transduction mechanism is based on the change in the electrical resistance of self-adjusting VACNTs in contact with each other. The confined growth of VACNTs enables their facile integration with fully fabricated microstructures. Experimental investigation revealed that the proposed displacement sensor is outstandingly sensitive, a characteristic that originates from the drastic changes in the electrical resistance of the contacting CNT arrays for small displacements. Furthermore, multidirectional sensing was achieved by combining different sensing modes with a cost-effective batch fabrication process (a concept that can be easily integrated with other nano- and microdevices). As an exemplary mechanical sensor utilizing the proposed displacement transduction, we demonstrated a 3-axis accelerometer characterized by high sensitivity and high resonant frequency. Considering that most micromechanical sensors such as accelerometers, gyroscopes, pressure sensors, and strain gauges are operated by mechanically movable structures within the displacement range of a few micrometers, the proposed displacement sensing mechanism is not only applicable to the demonstrated 3-axis accelerometer but can also be used for diverse micromechanical sensors to enhance the sensitivity with simple circuitry of resistive type sensors.

EXPERIMENTAL SECTION

The silicon microstructures of the VACNT-based displacement sensor were fabricated on silicon-on-insulator (SOI) wafers using a heavily doped device layer. Subsequent to the lithographic patterning of the etch masks on the front and back sides of the SOI wafers, the device and handle layers were etched by deep reactive ion etching. The remaining etch mask layers were then etched, and the exposed buried oxide layer was removed to release the movable structure. An iron catalyst layer of thickness 5 nm was thereafter deposited by electron beam evaporation. The patterning of the catalyst layer was done using a separately prepared shadow mask. The VACNT arrays were then synthesized by thermal chemical vapor deposition. The silicon microstructures with the catalyst layer were heated to 700 °C in a nitrogen-filled furnace. After pretreatment in a 100 sccm flow of ammonia for 30 min, a 50 sccm flow of acetylene was introduced to initiate carbon nucleation. The VACNTs were then grown for 15 min. The detailed fabrication procedure and some illustrations are presented in the Supporting Information.

ASSOCIATED CONTENT

Supporting Information

Detailed fabrication process of VACNT-based displacement sensor; comparison of sensitivities of the proposed VACNT-based displacement sensor and a piezoresistive sensor; linear output current signal in the sliding mode; sensitivity and maximum sensing range in the sliding mode; design and demonstration of 1-axis accelerometer; sensing modes and changes in contact resistance for accelerations in different directions; comparison of performance of proposed 3-axis accelerometer with those of piezoresistive accelerometers of previous studies. This material is available free of charge via the Internet at http://pubs.acs.org.

AUTHOR INFORMATION

Corresponding Author

*J. Kim. E-mail: kimjb@yonsei.ac.kr.

Notes

The authors declare no competing financial interest.

ACKNOWLEDGMENTS

This work was supported by the Center for Integrated Smart Sensors funded by the Ministry of Science, ICT & Future Planning as Global Frontier Project (CISS-2012M3A6A6054201) and the Pioneer Research Center Program through the National Research Foundation of Korea funded by the Ministry of Science, ICT & Future Planning (NRF-2010-0019459).

REFERENCES

(1) Sun, Y.; Nelson, B. J.; Potasek, D. P.; Enikov, E. A Bulk Microfabricated Multi-Axis Capacitive Cellular Force Sensor using Transverse Comb Drives. *J. Micromech. Microeng.* **2002**, *12*, 832−840.

(2) Mannsfeld, S. C. B.; Tee, B. C.-K.; Stoltenberg, R. M.; Chen, C. V. H.-H.; Barman, S.; Muir, B. V. O.; Sokolov, A. N.; Reese, C.; Bao, Z. Highly Sensitive Flexible Pressure Sensors with Microstructured Rubber Dielectric Layers. *Nat. Mater.* **2010**, *9*, 859−864.

(3) Li, X. X.; Bao, M. H.; Yang, H.; Shen, S. Q.; Lu, D. R. A Micromachined Piezoresistive Angular Rate Sensor with a Composite Beam Structure. *Sens. Actuators, A* **1999**, *72*, 217−223.

(4) Roylance, L. M.; Angell, J. B. A Batch-fabricated Silicon Accelerometer. *IEEE Trans. Electron Devices* **1979**, *26*, 1911−1917.

(5) Wang, Y.-H.; Lee, C.-Y.; Chiang, C.-M. A MEMS-based Air Flow Sensor with a Free-Standing Microcantilever Structure. *Sensors* **2007**, *7*, 2389−2401.

(6) Engel, J.; Chen, J.; Liu, C. Development of Polyimide Flexible Tactile Sensor Skin. *J. Micromech. Microeng.* **2003**, *13*, 359−366.

(7) Yazdi, N.; Ayazi, F.; Najafi, K. Micromachined Inertial Sensors. *Proc. IEEE* **1998**, *86*, 1640−1659.

(8) Ruoff, R. S.; Lorents, D. C. Mechanical and Thermal-Properties of Carbon Nanotubes. *Carbon* **1998**, *33*, 925−930.

(9) Treacy, M. M. J.; Ebbesen, T. W.; Gibson, J. M. Exceptionally High Young's Modulus Observed for Individual Carbon Nanotubes. *Nature (London, U. K.)* **1996**, *381*, 678−680.

(10) Yu, M. F.; Lourie, O.; Dyer, M. J.; Moloni, K.; Kelly, T. F.; Ruoff, R. S. Strength and Breaking Mechanism of Multiwalled Carbon Nanotubes under Tensile Load. *Science (Washington, DC, U. S.)* **2000**, *287*, 637−640.

(11) Dai, H. J.; Wong, E. W.; Lieber, C. M. Probing Electrical Transport in Nanomaterials: Conductivity of Individual Carbon Nanotubes. *Science (Washington, DC, U. S.)* **1996**, *272*, 523−526.

(12) Javey, A.; Guo, J.; Wang, Q.; Lundstrom, M.; Dai, H. Ballistic Carbon Nanotube Field-Effect Transistors. *Nature (London, U. K.)* **2003**, *424*, 654−657.

(13) Guo, L. Q.; Wang, R.; Xu, H. M.; Liang, J. Wear-Resistance Comparison of Carbon Nanotubes and Conventional Silicon-Probes for Atomic Force Microscopy. *Wear* **2005**, *258*, 1836−1839.

(14) Stampfer, C.; Jungen, A.; Linderman, R.; Obergfell, D.; Roth, S.; Hierold, C. Nano-Electromechanical Displacement Sensing Based on Single-Walled Carbon Nanotubes. *Nano Lett.* **2006**, *6*, 1449−1453.

(15) Chang, N. K.; Su, C. C.; Chang, S. H. Fabrication of Single-Walled Carbon Nanotube Flexible Strain Sensors with High Sensitivity. *Appl. Phys. Lett.* **2008**, *92*, 063501.

(16) Grow, R. J.; Wang, Q.; Cao, J.; Wang, D. W.; Dai, H. Piezoresistance of Carbon Nanotubes on Deformable Thin-Film Membranes. *Appl. Phys. Lett.* **2005**, *86*, 093104.

(17) Tombler, T. W.; Zhou, C.; Alexseyev, L.; Kong, J.; Dai, H.; Liu, L.; Jayanthi, C. S.; Tang, M.; Wu, S. Reversible Electromechanical

Characteristics of Carbon Nanotubes under Local-Probe Manipulation. *Nature (London, U. K.)* **2000**, *405*, 769−772.
(18) Cao, A. Y.; Dickrell, P. L.; Sawyer, W. G.; Ghasemi-Nejhad, M. N.; Ajayan, P. M. Super-Compressible Foamlike Carbon Nanotube Films. *Science (Washington, DC, U. S.)* **2005**, *310*, 1307−1310.
(19) Suhr, J.; Victor, P.; Ci, L.; Sreekala, S.; Zhang, X.; Nalamasu, O.; Ajayan, P. M. Fatigue Resistance of Aligned Carbon Nanotube Arrays under Cyclic Compression. *Nat. Nanotechnol.* **2007**, *2*, 417−421.
(20) Lee, B. Y.; Heo, K.; Bak, J. H.; Cho, S. U.; Moon, S.; Park, Y. D.; Hong, S. Scalable Assembly Method of Vertically-Suspended and Stretched Carbon Nanotube Network Devices for Nanoscale Electro-Mechanical Sensing Components. *Nano Lett.* **2008**, *8*, 4483−4487.
(21) Pushparaj, V. L.; Ci, L.; Sreekala, S.; Kumar, A.; Kesapragada, S.; Gall, D.; Nalamasu, O.; Pulickel, A. M.; Suhr, J. Effects of Compressive Strains on Electrical Conductivities of a Macroscale Carbon Nanotube Block. *Appl. Phys. Lett.* **2007**, *91*, 153116.
(22) Bsoul, A.; Ali, M. S. M.; Nojeh, A.; Takahata, K. Piezoresistive Strain Sensing using Carbon Nanotube Forests Suspended by Parylene-C Membranes. *Appl. Phys. Lett.* **2012**, *100*, 213510.
(23) Yilmazoglu, O.; Popp, A.; Pavlidis, D.; Schneider, J. J.; Garth, D.; Schuttler, F. Battenberg, G. Vertically Aligned Multiwalled Carbon Nanotubes for Pressure, Tactile and Vibration Sensing. *Nanotechnology* **2012**, *23*, 085501.
(24) Cola, B. A.; Xu, J.; Fisher, T. S. Contact Mechanics and Thermal Conductance of Carbon Nanotube Array Interfaces. *Int. J. Heat Mass Transfer* **2009**, *52*, 3490−3503.
(25) Choi, J.; Lee, J.; Eun, Y.; Kim, M.; Kim, J. Aligned Carbon Nanotube Arrays for Degradation-Resistant, Intimate Contact in Micromechanical Devices. *Adv. Mater.* **2011**, *19*, 2231−2236.
(26) Bedewy, M.; Meshot, E. R.; Guo, H.; Verploegen, E. A.; Lu, W.; Hart, A. J. Collective Mechanism for the Evolution and Self-Termination of Vertically Aligned Carbon Nanotube Growth. *J. Phys. Chem. C* **2009**, *113*, 20576−20582.
(27) Hart, A. J.; Slocum, A. H. Force Output, Control of Film Structure, and Microscale Shape Transfer by Carbon Nanotube Growth under Mechanical Pressure. *Nano Lett.* **2006**, *6*, 1254−1260.
(28) Cao, A.; Baskaran, R.; Frederick, M. J.; Turner, K.; Ajayan, P. M.; Ramanath, G. Direction-Selective and Length-Tunable In-Plane Growth of Carbon Nanotubes. *Adv. Mater.* **2003**, *15*, 1105−1109.
(29) Bower, C.; Zhou, O.; Zhu, W.; Werder, D. J.; Jin, S. H. Nucleation and Growth of Carbon Nanotubes by Microwave Plasma Chemical Vapor Deposition. *Appl. Phys. Lett.* **2000**, *77*, 2767−2769.
(30) Kovacs, G. T. A. *Micromachined transducers sourcebook*; WCB/McGraw-Hill: NewYork, 1998; Chapter 5, pp 210−275.
(31) Legtenberg, R.; Groeneveld, A. W.; Elwenspoek, M. Comb-Drive Actuators for Large Displacements. *J. Micromech. Microeng.* **1996**, *6*, 320−329.
(32) Allaoui, A.; Hoa, S. V.; Evesquea, P.; Bai, J. Electronic Transport in Carbon Nanotube Tangles under Compression: The Role of Contact Resistance. *Scr. Mater.* **2009**, *61*, 628−631.
(33) Allaoui, A.; Hoa, S. V.; Pugh, M. D. The Electronic Transport Properties and Microstructure of Carbon Nanofiber/Epoxy Composites. *Compos. Sci. Technol.* **2008**, *68*, 410−416.
(34) Wang, S.; Liang, Z.; Wang, B.; Zhang, C. Statistical Characterization of Single-Wall Carbon Nanotube Length Distribution. *Nanotechnology* **2006**, *17*, 634−639.